Physics in Medicine & Biology

PAPER

Quantitative performance evaluation of ^{124}I PET/MRI lesion dosimetry in differentiated thyroid cancer

To cite this article: R Wierts *et al* 2018 *Phys. Med. Biol.* **63** 015014

IOP Publishing Phys. Med. Biol. 63 (2018) 015014 (10pp) https://doi.org/10.1088/1361-6560/aa990b

Physics in Medicine & Biology

IPEM Institute of Physics and Engineering in Medicine

PAPER

Quantitative performance evaluation of ^{124}I PET/MRI lesion dosimetry in differentiated thyroid cancer

R Wierts[1], W Jentzen[2], H H Quick[3,4], H J Wisselink[5], I N A Pooters[1], J E Wildberger[1], K Herrmann[2], G J Kemerink[1], W H Backes[1] and F M Mottaghy[1,6]

[1] Department of Radiology and Nuclear Medicine, Maastricht University Medical Centre, P. Debyelaan 25, 6229 HX, Maastricht, Netherlands
[2] Department of Nuclear Medicine, University Hospital Essen, Hufelandstrasse 55, D-45122, Essen, Germany
[3] High Field and Hybrid MR Imaging, University Hospital Essen, Hufelandstrasse 55, D-45147, Essen, Germany
[4] Erwin L. Hahn Institute for MR Imaging, University of Duisburg-Essen, Kokereiallee 7, D-45141, Essen, Germany
[5] Technical Medicine, University of Twente, Drienerlolaan 5, 7522 NB, Enschede, Netherlands
[6] Department of Nuclear Medicine, University Hospital RWTH Aachen University, Pauwelsstrasse 30, D-52074, Aachen, Germany

E-mail: roel.wierts@mumc.nl

RECEIVED
21 July 2017

REVISED
30 October 2017

ACCEPTED FOR PUBLICATION
8 November 2017

PUBLISHED
19 December 2017

Keywords: PET/MRI, ^{124}I, lesion dosimetry, radioiodine therapy, thyroid carcinoma

Supplementary material for this article is available online

Abstract

The aim was to investigate the quantitative performance of ^{124}I PET/MRI for pre-therapy lesion dosimetry in differentiated thyroid cancer (DTC). Phantom measurements were performed on a PET/MRI system (Biograph mMR, Siemens Healthcare) using ^{124}I and ^{18}F. The PET calibration factor and the influence of radiofrequency coil attenuation were determined using a cylindrical phantom homogeneously filled with radioactivity. The calibration factor was 1.00 ± 0.02 for ^{18}F and 0.88 ± 0.02 for ^{124}I. Near the radiofrequency surface coil an underestimation of less than 5% in radioactivity concentration was observed. Soft-tissue sphere recovery coefficients were determined using the NEMA IEC body phantom. Recovery coefficients were systematically higher for ^{18}F than for ^{124}I. In addition, the six spheres of the phantom were segmented using a PET-based iterative segmentation algorithm. For all ^{124}I measurements, the deviations in segmented lesion volume and mean radioactivity concentration relative to the actual values were smaller than 15% and 25%, respectively. The effect of MR-based attenuation correction (three- and four-segment μ-maps) on bone lesion quantification was assessed using radioactive spheres filled with a K_2HPO_4 solution mimicking bone lesions. The four-segment μ-map resulted in an underestimation of the imaged radioactivity concentration of up to 15%, whereas the three-segment μ-map resulted in an overestimation of up to 10%. For twenty lesions identified in six patients, a comparison of ^{124}I PET/MRI to PET/CT was performed with respect to segmented lesion volume and radioactivity concentration. The interclass correlation coefficients showed excellent agreement in segmented lesion volume and radioactivity concentration (0.999 and 0.95, respectively). In conclusion, it is feasible that accurate quantitative ^{124}I PET/MRI could be used to perform radioiodine pre-therapy lesion dosimetry in DTC.

1. Introduction

Radioiodine therapy, after total thyroidectomy, is the standard adjuvant therapy in differentiated thyroid cancer (DTC) (Cooper *et al* 2009). The radiation absorbed dose delivered to thyroid remnants and lesions (lymph nodes or distant metastases) is considered the most relevant quantity that has been shown to correlate with treatment outcome (Jentzen *et al* 2014). In recent decades, several groups have investigated the use of ^{124}I PET(/CT) to assess the lesion absorbed dose delivered in radioiodine therapy (Sgouros *et al* 2004, Jentzen *et al* 2008). In fact, ^{124}I PET/CT is considered the most accurate method for pre-therapy dosimetry assessment in DTC and has been shown to alter patient management (Freudenberg *et al* 2007) and to provide prognostic information on lesion response (Wierts *et al* 2016).

Reliable lesion dosimetry requires the accurate quantification of lesion volume and ^{124}I uptake at different time points. As a result of the limited soft-tissue contrast, the boundary of tumours and thyroid remnants can generally not be segmented clearly on CT. Therefore, lesion volume segmentation is commonly performed on PET images. However, due to the limited spatial resolution of PET, lesion volume determination, and therefore accurate lesion dosimetry, is only achieved in 25–40% of all iodine avid lesions (Jentzen *et al* 2014, Wierts *et al* 2016).

As a result of the superior soft-tissue contrast of MRI over CT, MRI may provide additional diagnostic information in DTC patients. Due to this superiority, Nagarajah *et al* (2011) concluded that PET/MRI can enhance diagnostic certainty for small lesions and improve pre-therapy lesion dosimetry in DTC. However, whereas CT-based PET attenuation correction is straightforward, MR-based attenuation correction is more challenging, particularly for bony structures (Schulz *et al* 2011, Aznar *et al* 2014). Moreover, the presence of radiofrequency (RF) surface coils in the PET field of view (FOV) can degrade PET image quantification (Delso *et al* 2010).

In general, the quantitative performance of PET/MRI systems is assessed for ^{18}F as this is the most commonly used PET radionuclide in clinical practice and is readily available. In contrast to ^{18}F, which is a pure positron (β^+) emitter (β^+: yield 97%, end-point energy: 0.63 MeV), ^{124}I PET quantification has been shown to be more difficult, mainly due to the higher positron energies (β_1^+: 10.7%, 2.1 MeV; β_2^+: 11.7%, 1.5 MeV) emitted by ^{124}I and the prompt gamma photons (0.603 MeV) emitted in cascade with approximately half of the positrons (Jentzen *et al* 2011), producing so-called prompt gamma coincidences. Although recently the Biograph mMR PET/MRI system image quality of ^{124}I was assessed and compared to ^{18}F (Soderlund *et al* 2015), quantitative performance for lesion dosimetry in radioiodine treatment has not yet been investigated.

The aim of this study was to investigate the quantitative performance characteristics of PET/MRI with respect to ^{124}I PET lesion dosimetry in radioiodine therapy in DTC patients.

2. Materials and methods

2.1. PET/MRI system

PET/MRI measurements were performed on a 3 T Biograph mMR system with a gradient system with a maximum amplitude of 45 mT m^{-1} and a maximum slew rate of 200 (T/m) s^{-1} (Siemens Healthcare GmbH, Erlangen, Germany, software version VB20P). PET images were reconstructed using the manufacturer's 3D iterative ordinary Poisson ordered-subsets expectation maximization (OP-OSEM3D) reconstruction algorithm. Unless mentioned otherwise, the default manufacturer's recommendations for image reconstruction were applied: 3 iterations and 21 subsets, cuboid-shaped voxels of 2.0 mm and a 4.0 mm Gaussian smoothing filter. Correction of ^{124}I prompt gamma coincidences were performed using the standard manufacturer's reconstruction software (Hayden *et al* 2011).

For attenuation and scatter correction in patients, in general a four-segment (air, lung, fat and soft tissue) attenuation map (μ-map) derived from a 3D Dixon-VIBE MR sequence was used. For head–neck imaging, the system provides an alternative three-segment (air, soft-tissue and bone) μ-map, using an ultrashort echo-time (UTE) MR sequence. For quantitative PET phantom measurements a CT-based (Gemini TF PET/64-slice CT scanner, Philips) μ-map was used for PET attenuation and scatter correction (Ziegler *et al* 2015).

2.2. Radionuclides

All phantom measurements were performed with ^{124}I-sodium iodide (^{124}I-NaI) and compared to ^{18}F-fluorodeoxyglucose (^{18}F-FDG).

Measurement of the absolute ^{124}I activity is crucial for dosimetry quantification and requires a standardized procedure (Jentzen *et al* 2008, Jentzen 2010). The radioactivity measurement of syringes used for phantom preparation was performed using a dose calibrator (Isomed 2010, MED, Dresden) that was validated against a high-purity germanium semiconductor detector (GR1018, Canberra Industries, Connecticut).

2.3. Quantitative performance measurements

2.3.1. Calibration factor (CF) and RF coil attenuation

The PET calibration factor was determined using a cylindrical phantom (internal diameter 14 cm, internal length 20 cm) homogeneously filled with radioactivity in aqueous solution. Single-bed PET acquisitions of 7 min were performed using a radioactivity concentration of 6.5 kBq ml^{-1} for ^{18}F, corresponding to the FDG PET/CT standard operating procedures for quality control of the European association of nuclear medicine (EANM) (Boellaard *et al* 2010). As in clinical practice, lower amounts of ^{124}I are administered compared to ^{18}F; an activity concentration of 1.70 kBq ml^{-1} was used for ^{124}I. As the CF measurement uncertainty is increased for lower counting statistics, PET acquisition times of 120 min were used to obtain similar counting statistics to those for the ^{18}F measurements, taking into account both the lower activity concentration and lower positron yield of ^{124}I. For both ^{18}F and ^{124}I, measurements were first performed without RF coils as a reference.

To investigate the influence of attenuation of two commercially available Biograph mMR PET-compatible RF coils used for head–neck imaging, the phantom measurements were repeated twice: the first time with the cylindrical phantom placed inside the rigid 16-channel head–neck RF coil, the second time with the small and flexible four-channel special-purpose surface RF coil placed on top of the cylindrical phantom.

For all measurements with and without RF coils, the PET calibration factor *CF* was determined as the mean radioactivity concentration a_{mean} measured in a central cylindrical volume of interest (VOI) (diameter 10 cm, length 15 cm), divided by the prepared or true radioactivity concentration a_{true}:

$$CF = \frac{a_{mean}}{a_{true}}. \quad (1)$$

The standard deviation (SD) of the *CF* was determined as the standard deviation of the *CF* calculated for the individual transversal slices, using a circular region of interest with a diameter of 10 cm. Furthermore, for each axial plane five circular regions of interest (ROIs) with a radius of 1.0 cm were drawn as shown in figure 1(a). For each ROI and plane number, the ratio of the mean radioactivity concentration measured with RF coil relative to the reference measurement without RF coil was calculated. From these calculated radioactivity concentration ratios, the mean and standard deviation were determined. The 95% uncertainty interval of the radioactivity concentration ratio per plane was calculated as the mean ratio $\pm$ 2 standard deviations.

2.3.2. *Recovery coefficients using a soft-tissue phantom*

Soft-tissue sphere recovery coefficients (RCs) were determined using the NEMA IEC body phantom. This phantom consists of a torso-shaped background compartment containing six fillable spheres (diameter: 10, 13, 17, 22, 28 and 37 mm) and a cylindrical insert filled with polystyrene (internal diameter 44.5 mm). Corresponding to the EANM standard operating procedures for quality control of FDG PET/CT (Boellaard *et al* 2010), all spheres were homogeneously filled with an aqueous solution with a radioactivity concentration of 13.8 kBq ml^{-1} for ^{18}F and 14.0 kBq ml^{-1} for ^{124}I. For both radionuclides, measurements were performed without radioactivity present in the background compartment (cold background). In addition, measurements were performed with radioactivity present in the background compartment (hot background), corresponding to a prepared sphere-to-background ratio of 10:1. For accurate assessment of the RC, single-bed PET high counting statistic acquisitions of 30 min for ^{18}F and 60 min for ^{124}I were performed. The emission time of the ^{124}I measurements was doubled with respect to ^{18}F to (partly) correct for the lower positron yield of ^{124}I.

The mean and maximum radioactivity concentrations were determined by drawing spherical VOIs with a diameter corresponding to the actual sphere diameter. The mean (maximum) recovery coefficients (*RC*) were calculated by dividing the measured mean (maximum) sphere radioactivity concentration C_{meas} by the prepared or true sphere radioactivity concentration C_{true}:

$$RC = \frac{C_{meas}}{C_{true}}. \quad (2)$$

2.3.3. *Effect of MR-based attenuation correction of bone lesions*

The simulation of bone lesions was performed with a bone-tissue phantom by filling the six spheres of the NEMA IEC body phantom with a K_2HPO_4 solution mixed with ^{18}F or ^{124}I. For both radionuclides, a high and low concentration of K_2HPO_4, simulating compact and cancellous bone tissue, was used: 0.84 g ml^{-1} and 0.42 g ml^{-1}, resulting in CT numbers of 780 HU and 490 HU, respectively. For the high and low concentrations of K_2HPO_4, the radioactivity concentration and acquisition time (within parentheses) was 9.3 kBq ml^{-1} (30 min) and 18.8 kBq ml^{-1} (15 min) for ^{18}F and 27.9 kBq ml^{-1} (20 min) and 14.9 kBq ml^{-1} (40 min) for ^{124}I, respectively. The radioactivity concentrations and acquisition times were chosen to obtain similar high counting statistics for the low and high K_2HPO_4 concentration measurements for each radionuclide separately, partly compensating for the lower positron yield of ^{124}I compared to ^{18}F.

PET images were reconstructed using three different μ-maps. First, reference PET images were reconstructed using an original CT-based μ-map of the bone-tissue phantom. Second, to simulate the four-segment MR-based attenuation correction, in which bone is (incorrectly) classified as soft-tissue, the linear attenuation coefficient of the bony spheres in the original CT-based μ-map was set to that of water. PET images were reconstructed using this adapted μ-map. Third, the three-segment MR-based attenuation correction was simulated by replacing the linear attenuation correction of the bony spheres with a fixed linear attenuation coefficient of 0.151 cm^{-1}. PET reconstructions were performed using the adapted μ-map.

Spherical VOIs corresponding to the actual sphere dimensions were drawn for all spheres. The percentage deviation in mean radioactivity concentration measured in the reconstructed images using the three- or four-segment MR-based μ-map relative to the reference PET images was calculated.

2.4. PET-based lesion segmentation

2.4.1. Lesion segmentation method

For reliable lesion dosimetry, accurate volume segmentation of the lesion and its radioactivity concentration are required. In a recent ^{124}I PET/CT study, reliable lesion dosimetry was achieved using a PET-based iterative thresholding algorithm (Wierts *et al* 2016). The method uses the average lesion activity concentration assuming a spherically shaped lesion with a homogeneous radioactivity concentration (Jentzen 2015). Accounting for the full-width-at-half-maximum (FWHM) spatial resolution of the PET images and background radioactivity level, the segmentation algorithm determines the optimum threshold value for lesion delineation. Besides lesion volume, the method calculates the lesion mean radioactivity concentration, corrected for partial volume effects (Jentzen 2015).

2.4.2. PET spatial resolution measurement

The described volume segmentation method requires the effective spatial resolution of the PET images. Therefore, the spatial resolution was measured using a line-source phantom consisting of a cylindrical phantom (diameter 20 cm, length 30 cm) filled with water in which a plastic line source was placed (internal diameter 0.9 mm, length 25 cm). Tangential and radial resolution were measured at 1, 10 and 20 cm distance to the centre of the FOV. Axial resolution was measured at the centre of the FOV and at 9 cm offset. The radioactivity concentration of the line sources was 10 MBq ml^{-1} for ^{18}F and 8 MBq ml^{-1} for ^{124}I using an acquisition time of 30 min and 60 min. Except for a 2.0 mm Gaussian smoothing filter, default PET reconstruction settings were used.

For each direction (tangential, radial, axial), the FWHM spatial resolution was calculated by fitting a Gaussian curve through the radioactivity profile of the reconstructed line source using Matlab (The MathWorks Inc.). The average spatial resolution was calculated from the spatial resolution values measured at different distances from the centre of the FOV for each direction. Finally, the effective spatial resolution was calculated as the mean value of the average spatial resolution of the three directions.

2.4.3. Lesion volume and radioactivity concentration assessment

The accuracy of the described PET-based iterative segmentation method was investigated for the soft-tissue phantom measurements. To this end, the iterative segmentation method was applied to all spheres using an Matlab script developed in-house. As the segmentation method uses the determined effective spatial resolution, the images were reconstructed with the same reconstruction settings as the spatial resolution measurements. The percentage deviation in segmented lesion volume and mean radioactivity concentration, corrected for partial volume effect, relative to the actual sphere volume and radioactivity concentration were determined.

2.5. Clinical ^{124}I PET/MRI lesion quantification using PET/CT as reference

Five DTC patients, who underwent both ^{124}I PET/CT (Biograph mCT, Siemens Healthcare GmbH, Erlangen, Germany) and ^{124}I PET/MRI were analyzed. All patients received total thyroidectomy prior to ^{124}I PET imaging. Patient preparation was performed by thyroid hormone withdrawal or recombinant human thyroid stimulating hormone. PET/CT acquisition was performed 24 h after oral administration of approximately 25 MBq ^{124}I, followed within 2 h by PET/MRI acquisition. Patients provided written informed consent to undergo the examinations, and the study was approved by the local ethics research committee.

PET/CT scans were acquired from head to thigh with arms up, using a low-dose CT scan (120 kVp, 15 mAs) and a PET emission time of 2 min/bed position typically used in clinical routine whole-body PET/CT examinations. In contrast, PET/MRI scans were restricted to the head–neck region with arms down. To achieve optimum PET image quality, PET acquisition was simultaneously performed for the duration of the MRI examinations, which contained a T_1-weighted VIBE sequence (echo time 2.46 ms, repetition time 6.18 ms, flip angle 12°), resulting in a long PET acquisition time of 20–30 min/bed position. PET image reconstructions were performed with the OP-OSEM3D reconstruction algorithm using 3 iterations, 24 subsets for PET/CT and 3 iterations, 21 subsets for PET/MRI. PET/CT and PET/MRI images had almost cuboid-shaped voxels of 2 mm. For both systems, correction for prompt gamma coincidences was applied for ^{124}I by the manufacturer (Hayden *et al* 2011). As the intrinsic PET spatial resolution of the PET/CT system is slightly lower than the PET/MRI system (5.5 mm versus 5.0 mm at zero smoothing level), different levels of Gaussian smoothing were applied (PET/CT 3.0 mm and PET/MRI 4.0 mm) to achieve almost identical effective spatial resolution (6.3 mm FWHM). As the five DTC patients did not show any bone lesions, additionally one neuro-endocrine patient was included, who was scanned with ^{124}I-meta-iodobenzylguanidine (^{124}I-MIBG) PET/MRI and PET/CT and showed multiple bone lesions.

With the exceptions of a higher administered activity of 45 MBq and a whole-body PET/MRI acquisition (5 min/bed position), PET acquisition and reconstruction settings were identical to those for the DTC patients.

Each ^{124}I avid lesion identified on both PET/CT and PET/MRI was segmented and the lesion volume and average radioactivity concentration was determined and compared using a Bland–Altman plot. In addition, the interclass correlation coefficient (ICC) was calculated (SPSS, version 23, IBM, Corp.).

3. Results

3.1. Quantitative performance measurements

3.1.1. Calibration factor and MRI coil attenuation

The calibration factors of ^{18}F and ^{124}I without RF coils were 1.00 ± 0.02 and 0.88 ± 0.02, respectively. For both the rigid head–neck coil (^{18}F: 1.02 ± 0.02, ^{124}I: 0.89 ± 0.02) and the flexible RF surface coil (^{18}F: 0.98 ± 0.02, ^{124}I: 0.88 ± 0.02) no substantial deviations of the calibration factor with respect to the reference measurement were observed.

Figure 1 shows the ratio of mean radioactivity concentration measurements with RF coil to the reference measurement without RF coil as a function of the axial plane number. As the ^{18}F and ^{124}I measurements showed comparable results, only the ^{124}I measurements are shown. ^{18}F data are shown in the supplementary material (stacks.iop.org/PMB/63/015014/mmedia). As can be seen in figure 1(a), for the head–neck RF coil no notable deviations of the mean radioactivity concentration with respect to the 95% uncertainty interval were observed for all circular ROIs, indicating that the automatic detection and attenuation correction for the head–neck RF coil worked properly. Figure 1(b) shows that at planes 35–60, corresponding to the location of the RF surface coil, a small decrease of 5% in mean radioactivity concentration ratio derived from the ROI situated in close proximity to the RF surface coil (ROI1). This decrease is explained by the fact that the PET attenuation caused by the RF surface coil was not taken into account in the attenuation correction during PET image reconstruction.

3.1.2. Recovery coefficients

In figure 2 the soft-tissue RC_{mean} and RC_{max} values are shown as a function of the sphere volume. No substantial differences were observed between the measurements with and without background radioactivity. The *RC* values of ^{18}F are systematically higher compared to those for ^{124}I. Although for ^{18}F the largest spheres reach an RC_{max} value of unity, for ^{124}I an underestimation of approximately 10% is observed. For ^{124}I larger underestimations of up to 38% in *RC* values with respect to ^{18}F are observed for the smallest sphere, most likely caused by the higher positron range of ^{124}I compared to ^{18}F, resulting in a larger partial volume effect. The centre slice images of the soft-tissue sphere phantom are shown in the supplementary material.

3.1.3. Effect of MR-based attenuation correction of bone lesions

Figure 3 presents the percentage deviation in mean ^{124}I radioactivity concentration of the bone lesion images using the three- or four-segment MR-based μ-map relative to the CT-based μ-map as a function of sphere diameter. The ^{18}F reconstructed images showed highly comparable results (supplementary material). Attenuation correction performed on the standard four-segment (without bone) MR-based μ-map resulted in an underestimation of up to 15% of the mean radioactivity concentration, due to the too low linear attenuation coefficient assigned to the bone lesion simulating spheres. This underestimation increased with increasing density and sphere diameter. In contrast, the three-segment (with bone) MR-based μ-map yielded an overestimation of up to 10%, indicating that a too high linear attenuation correction is assigned to the spheres. This overestimation increased with decreasing density and increasing sphere diameter.

3.1.4. PET spatial resolution measurement

The effective spatial resolutions of ^{18}F and ^{124}I were 4.3 ± 0.5 mm and 5.0 ± 0.3 mm. Compared to ^{18}F, the spatial resolution of ^{124}I was degraded as a result of the high-energy positrons of ^{124}I. The spatial resolution data for each direction are presented in table 1.

3.1.5. Lesion volume and radioactivity concentration assessment

Figure 4 shows the results of the lesion segmentation. For the ^{124}I phantom measurements, the errors in segmented lesion volume and partial volume corrected lesion activity concentration were less than 15% and 25%, respectively. Except for the smallest sphere, all segmented volumes were smaller for the measurements with, rather than without, background radioactivity.

3.2. Clinical ^{124}I PET/MRI lesion quantification compared to PET/CT

Twenty lesions (six lymph nodes, ten thyroid remnants and four bone metastases) were identified both on PET/MRI and PET/CT images. Two lesions (lymph nodes) showing very low ^{124}I uptake could only be identified on

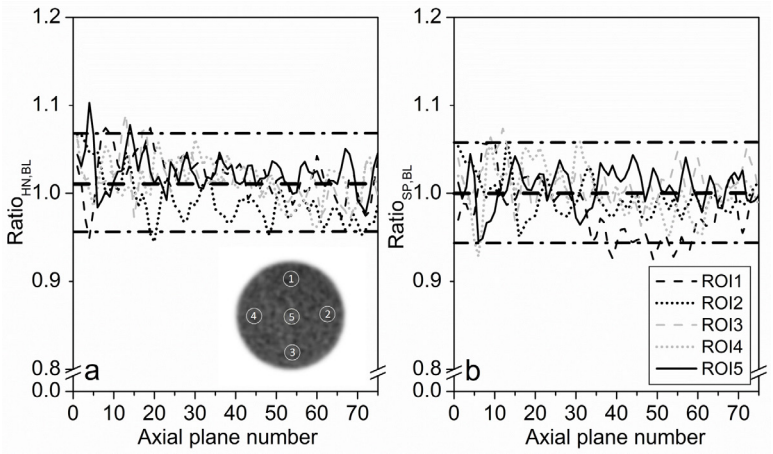

Figure 1. The influence of RF coil attenuation of the PET signal is assessed using the ratio of the mean ^{124}I radioactivity concentration with RF coil ((a) head–neck coil, (b) special purpose coil located between plane number 35 and 60) compared to the reference measurement without RF coil measured for all five ROIs shown in the insert of figure (a). The horizontal dashed and dash-dotted lines represent the average ratio and 95% uncertainty interval of the radioactivity concentration ratio per plane, respectively.

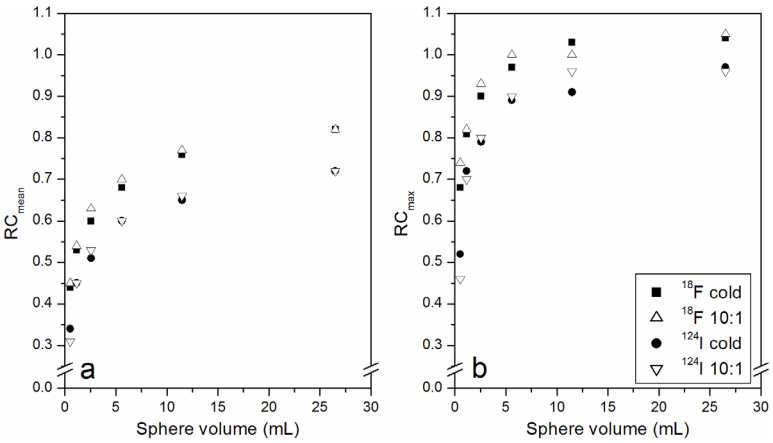

Figure 2. The accuracy of PET quantification for the soft-tissue phantom is investigated for both ^{18}F and ^{124}I by measuring the RC_{mean} (a) and RC_{max} (b) as a function of the sphere volume with and without background radioactivity.

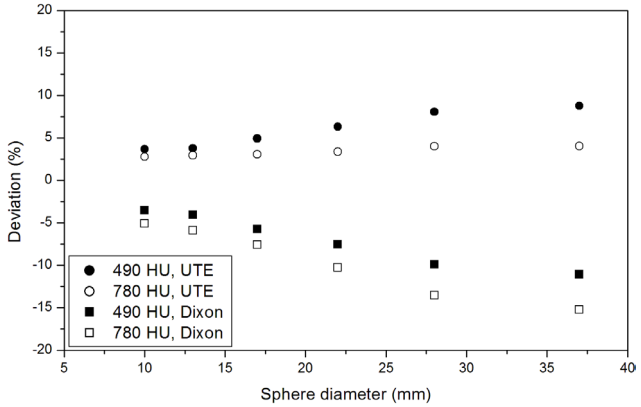

Figure 3. The effect of MR-based attenuation correction of bone simulating tissue is determined from the percentage deviation in measured mean ^{124}I radioactivity concentration using the three- (UTE) or four- (3D Dixon-vibe) segment MR-based μ-map with respect to the original CT-based μ-map as a function of the sphere diameter.

PET/MRI. As the PET/MRI acquisition was restricted to the head–neck region, one distant bone metastasis present in the lumbar spine region was only visualized in the whole-body PET/CT images. In figure 5 fused ^{124}I PET/CT and PET/MRI images of one patient are presented. In figure 6 the Bland–Altman plots comparing the segmented lesion volume and average radioactivity concentration measured with PET/CT and PET/MRI are shown.

Table 1. Spatial resolution measurement results.

Distance to CFOV (cm)	FWHM 18F (mm)	FWHM ^{124}I (mm)
Tangential spatial resolution		
1	3.57	4.24
10	4.16	4.62
20	4.40	4.85
Radial spatial resolution		
1	3.70	4.36
10	4.25	4.91
20	6.46	6.23
Axial spatial resolution		
1	3.99	5.18
9	3.87	5.21
Effective spatial resolution		
—	4.3 ± 0.5	5.0 ± 0.3

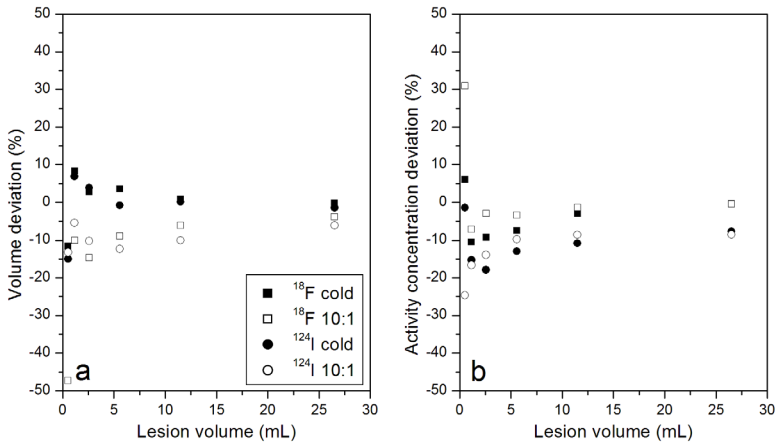

Figure 4. The accuracy of the used segmentation algorithm for the soft-tissue phantom is assessed from the percentage deviation in segmented lesion volume (a) and mean radioactivity concentration (b) as a function of sphere volume for both ^{18}F and ^{124}I with and without background radioactivity.

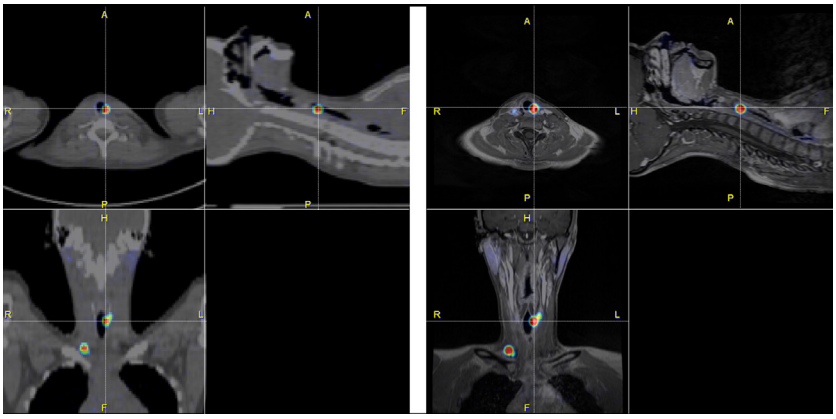

Figure 5. Visual depiction of clinical ^{124}I PET/CT (left) and PET/MRI (right) images of the same patient showing iodine avid lesions which could not be identified on CT on MRI images alone.

The ICC values revealed an excellent agreement between PET/MRI and PET/CT quantification for both lesion volume (0.999; 95%-confidence interval: (0.999–1.00)) and average radioactivity concentration (0.95; 95%-confidence interval (0.87–0.98)). However, percentage deviations larger than 25% in segmented lesion volume (radioactivity concentration) were observed for about 50% (25%) of the lesions, particularly for the small lesions (detailed information in supplementary material).

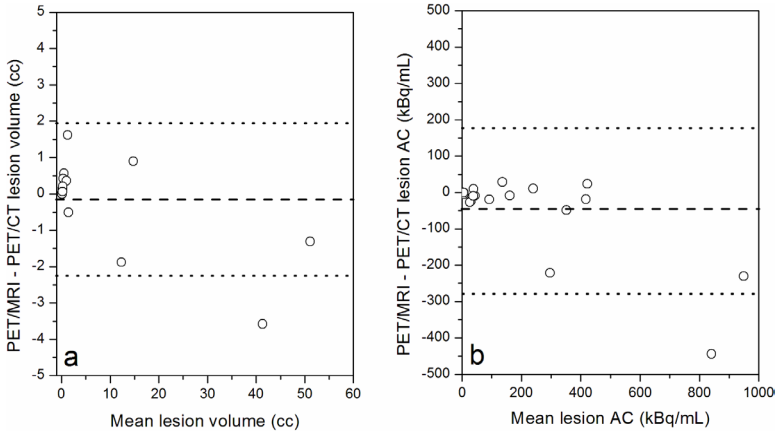

Figure 6. Comparison of ^{124}I PET/MRI lesion segmented volume (a) and average activity concentration (AC) compared to ^{124}I PET/CT in a clinical setting using Bland–Altman analysis. The dashed line represents the mean activity concentration difference between PET/MRI and PET/CT. The dotted lines represent the 95% confidence interval. Due to overlap of the symbols, less than the twenty analyzed lesions are distinguishable.

4. Discussion

To perform reliable ^{124}I PET/MRI lesion dosimetry in DTC patients, an accurate assessment of lesion uptake at different time points and lesion volume is required. In previous studies, a systematic underestimation of approximately 10% in measured ^{124}I radioactivity concentration has been reported compared to ^{18}F (Jentzen *et al* 2008, Gregory *et al* 2009, Jentzen 2010). This underestimation has in the literature been ascribed to the overestimation of the conventionally applied scatter correction algorithms resulting in an over-subtraction in the central part of the image (Conti and Eriksson 2016). To overcome this problem, a prompt-gamma correction method for ^{124}I, using a scaled random estimate matching the tails of the prompt sinogram (Hayden *et al* 2011), is by default implemented on the Siemens Biograph mMR and Biograph mCT systems. However, for both the calibration factor and soft-tissue sphere *RC* measurements, we still observe an underestimation of 10–12% in measured radioactivity concentration compared to ^{18}F. Although Preylowski *et al* (2013) showed that implementation of the prompt-gamma correction method did not result in a notable increase in ^{124}I *RC* values for the Biograph mCT system, they reported similar *RC* values for ^{124}I and ^{18}F, in contrast to our results. This discrepancy cannot be completely resolved, but is most likely related to an imprecise ^{124}I calibration factor of the dose calibrator (Jentzen *et al* 2008, Jentzen 2010, Beattie *et al* 2014).

For high resolution MR imaging of the head–neck region, the use of dedicated head–neck and RF surface coils is essential in clinical practice. Such coils cause attenuation of the PET signal, resulting in significant underestimation of the measured radioactivity concentration of up to 19% (Delso *et al* 2010, Eldib *et al* 2015). For rigid, stationary coils, such as the head–neck coil, a CT-based μ-map of the coil is automatically integrated in the PET image reconstruction algorithm upon connection and placement of the coil on the PET/MRI system. Although for flexible surface coils various techniques for attenuation correction have been proposed (Paulus *et al* 2012, Eldib *et al* 2015), all Biograph mMR surface coils, including the small and flexible four-channel RF coil used in this study, are optimized for PET-transparency by stripping the coils from as much of its PET attenuation materials as possible. Our results show that the effect of both investigated RF coils on the PET quantification was locally smaller than 5% for both ^{18}F and ^{124}I.

The classification of bone as soft-tissue in the standard four-segment μ-map resulted in an increasing underestimation of the measured radioactivity concentration of up to 15% with increasing sphere density and diameter, in agreement with values reported in the literature (Aznar *et al* 2014, Paulus *et al* 2015). In contrast, for the UTE three-segment μ-map, in which bone is assigned a fixed linear attenuation coefficient of 0.151 cm^{-1}, an increasing overestimation of up to 10% was found. A similar overestimation of bone using UTE-based μ-maps has also been reported in the literature (Berker *et al* 2012, Aasheim *et al* 2015). Recently, a novel MR-based attenuation correction technique using bone mask pairs for major bones has shown to improve PET/MR quantification in bone (Paulus *et al* 2015, Koesters *et al* 2016). Although the quantification differences for bone tissues are relatively small compared to other uncertainties in the dosimetry calculations (for instance, uncertainties in dose calibrator measurements, kinetic model used to estimate residence time, segmented lesion volume and mean radioactivity concentration), the effect of MR-based attenuation correction on ^{124}I lesion dosimetry of bone lesions requires further investigation.

The lesion segmentation technique used requires the PET spatial resolution to account for regional spill-out and spill-in effects. Therefore, the effective PET spatial image resolution was assessed using line sources in water

for both ^{18}F and ^{124}I. The spatial resolution of ^{124}I (5.0 mm) was 0.7 mm degraded compared to ^{18}F (4.3 mm), as a result of the high-energy positrons emitted by ^{124}I, in good agreement with reported ^{124}I PET/CT spatial resolution measurements (Jentzen *et al* 2008, Gregory *et al* 2009, Preylowski *et al* 2013). In contrast, using point sources in air, Soderlund *et al* (2015) reported equal ^{124}I and ^{18}F PET spatial resolution values for the Biograph mMR. This discrepancy is explained by the difference in positron range in measurement setup between a point source in water and air, shown by Kemerink *et al* (2011).

In the presence of background radioactivity, smaller lesion volumes were segmented than without background radioactivity for both ^{124}I and ^{18}F. This is explained by the effect of the cold lesion walls, which has been shown to result in a wall-related reduction of the optimum threshold value with increasing background (Hofheinz *et al* 2010). As a result of this effect, the applied segmentation threshold value is overestimated leading to an underestimation of lesion volume, in agreement with our observations. Despite this effect, the error in segmented lesion volume was less than 15% for ^{124}I. For ^{18}F a relatively large underestimation of 47% in segmented lesion volume was shown for the smallest sphere, which is probably caused by a combination of voxel discretization and the cold-wall effect. As this effect depends on the ratio of the thickness of the cold wall to the spatial resolution, this effect is more pronounced for ^{18}F than ^{124}I. Although the employed segmentation method used the average lesion activity concentration assuming a spherically shaped lesion with a homogeneous radioactivity concentration, accurate lesion segmentation was shown in clinical scenarios (Jentzen 2015).

For the ^{124}I and ^{18}F phantom measurements, the errors in partial volume corrected lesion activity concentration were less than 25%, with the exception of the smallest sphere for ^{18}F. Moreover, for ^{124}I the mean radioactivity concentration was systematically lower compared to ^{18}F, in agreement with the measured calibration factor and soft-tissue sphere RC. After correction for this effect, by dividing the measured radioactivity concentration by the calibration factor, the errors in the partial volume corrected lesion activity concentration were less than 15%. These errors are relatively small compared to other uncertainties in the dosimetry calculations mentioned previously.

Despite an excellent agreement in ^{124}I PET/MRI and PET/CT segmented lesion volume and radioactivity concentration according to the high ICC values (0.999 and 0.95, respectively), relatively large deviations were observed for some lesions, as shown in figure 6. This was caused by the low counting statistics of the PET/CT images, in particular for small lesions and lesions with low radioactivity concentration, and its noise was further enhanced by the 2 mm voxel size to avoid the volume discretization effect. Moreover, the differences in the PET emission times between PET/MRI and PET/CT was a limitation in the direct comparison of ^{124}I lesion quantification of the different modalities. This is reflected by two lymph nodes showing very low ^{124}I uptake. They could only be identified on the PET/MRI images as a result of the long emission time of the PET/MRI acquisition, indicating that an emission time of only 2 min used in whole-body PET/CT imaging may not be sufficient for identifying small lesions showing low ^{124}I uptake. However, the PET emission times used reflected the clinical practice. Specifically, in PET/CT, whole-body PET examinations are generally performed (with arms up) using an emission time per bed position of only a few minutes, whereas in PET/MRI, single bed positions of the head/neck region are typically performed (with arms down) as a result of the long acquisition times of the various MRI sequences used. As the PET acquisition can be performed simultaneously with MRI, the clinical PET acquisition time is matched to the time of the MRI examination to achieve the best PET image quality. Therefore, the quantitative comparison presented in this study provides a realistic representation of the use of ^{124}I PET/MRI in clinical routine for DTC.

Another shortcoming of this study was the small number of patients and analyzed lesions. Due to the absence of bone lesions in DTC patients, four ^{124}I-MIBG positive bone lesions were analyzed to study the effect of PET/MRI quantification for bone lesions. As the volume and radioactivity concentration of these lesions correspond to the values typically encountered in bone lesions in DTC patients, the comparison is considered to be representative for DTC patients.

5. Conclusion

For the rigid head–neck RF coil, no decrease in radioactivity concentration resulting from coil attenuation was observed. Near the RF surface coil, a small underestimation of less than 5% in radioactivity concentration was observed as a result of RF coil attenuation. For bone simulating lesions, MR-based attenuation correction using the four-segment μ-map resulted in an underestimation of the mean radioactivity concentration of up to 15%, whereas the use of the three-segment μ-map showed an overestimation of up to 10%. In a clinical setting, an excellent agreement between PET/MRI and PET/CT segmented lesion volume and mean ^{124}I radioactivity concentration was observed. Therefore, we conclude that accurate quantitative ^{124}I PET/MRI imaging with the aim of performing radioiodine pretherapy lesion dosimetry in DTC is feasible.

ORCID iDs

R Wierts https://orcid.org/0000-0002-9955-8754

References

Aasheim L B, Karlberg A, Goa P E, Haberg A, Sorhaug S, Fagerli U M and Eikenes L 2015 PET/MR brain imaging: evaluation of clinical UTE-based attenuation correction *Eur. J. Nucl. Med. Mol. Imaging* **42** 1439–46

Aznar M C, Sersar R, Saabye J, Ladefoged C N, Andersen F L, Rasmussen J H, Lofgren J and Beyer T 2014 Whole-body PET/MRI: the effect of bone attenuation during MR-based attenuation correction in oncology imaging *Eur. J. Radiol.* **83** 1177–83

Berker Y *et al* 2012 MRI-based attenuation correction for hybrid PET/MRI systems: a 4-class tissue segmentation technique using a combined ultrashort-echo-time/Dixon MRI sequence *J. Nucl. Med.* **53** 796–804

Boellaard R *et al* 2010 FDG PET and PET/CT: EANM procedure guidelines for tumour PET imaging: version 1.0 *Eur. J. Nucl. Med. Mol. Imaging* **37** 181–200

Beattie B J, Pentlow K S, O'Donoghue J and Humm J L 2014 A recommendation for revised dose calibrator measurement procedures for ^{89}Zr and ^{124}I *PLoS One* **9** e106868

Conti M and Eriksson L 2016 Physics of pure and non-pure positron emitters for PET: a review and a discussion *EJNMMI Phys.* **3** 8

Cooper D *et al* 2009 Revised american thyroid association management guidelines for patients with thyroid nodules and differentiated thyroid cancer *Thyroid* **19** 1167–214

Delso G, Martinez-Moller A, Bundschuh R A, Ladebeck R, Candidus Y, Faul D and Ziegler S I 2010 Evaluation of the attenuation properties of MR equipment for its use in a whole-body PET/MR scanner *Phys. Med. Biol.* **55** 4361–74

Eldib M, Bini J, Robson P M, Calcagno C, Faul D D, Tsoumpas C and Fayad Z A 2015 Markerless attenuation correction for carotid MRI surface receiver coils in combined PET/MR imaging *Phys. Med. Biol.* **60** 4705–17

Freudenberg L S, Jentzen W, Gorges R, Petrich T, Marlowe R J, Knust J and Bockisch A 2007 124I-PET dosimetry in advanced differentiated thyroid cancer: therapeutic impact *Nuklearmedizin* **46** 121–8

Gregory R A, Hooker C A, Partridge M and Flux G D 2009 Optimization and assessment of quantitative ^{124}I imaging on a philips gemini dual GS PET/CT system *Eur. J. Nucl. Med. Mol. Imaging* **36** 1037–48

Hayden C Jr, Casey M and Watson C 2011 Prompt gamma correction for non-standard isotopes in a PET scanner *US Patent* 7 894 652

Hofheinz F, Dittrich S, Potzsch C and Hoff J 2010 Effects of cold sphere walls in PET phantom measurements on the volume reproducing threshold *Phys. Med. Biol.* **55** 1099–113

Jentzen W 2010 Experimental investigation of factors affecting the absolute recovery coefficients in iodine-124 PET lesion imaging *Phys. Med. Biol.* **55** 2365–98

Jentzen W 2015 An improved iterative thresholding method to delineate PET volumes using the delineation-averaged signal instead of the enclosed maximum signal *J. Nucl. Med. Technol.* **43** 28–35

Jentzen W, Freudenberg L and Bockisch A 2011 Quantitative imaging of $^{(124)}$I with PET/CT in pretherapy lesion dosimetry effects impairing image quantification and their corrections *Q. J. Nucl. Med. Mol. Imaging* **55** 21–43

Jentzen W, Hoppenbrouwers J, Van Leeuwen P, Van der Velden D, Van de Kolk R, Poeppel T D, Nagarajah J, Brandau W, Bockisch A and Rosenbaum-Krumme S 2014 Assessment of lesion response in the initial radioiodine treatment of differentiated thyroid cancer using ^{124}I PET imaging *J. Nucl. Med.* **55** 1759–65

Jentzen W, Weise R, Kupferschlager J, Freudenberg L, Brandau W, Bares R, Burchert W and Bockisch A 2008 Iodine-124 PET dosimetry in differentiated thyroid cancer: recovery coefficient in 2D and 3D modes for PET(/CT) systems *Eur. J. Nucl. Med. Mol. Imaging* **35** 611–23

Kemerink G J, Visser M G, Franssen R, Beijer E, Zamburlini M, Halders S G, Brans B, Mottaghy F M and Teule G J 2011 Effect of the positron range of 18F, 68Ga and 124I on PET/CT in lung-equivalent materials *Eur. J. Nucl. Med. Mol. Imaging* **38** 940–8

Koesters T, Friedman K P, Fenchel M, Zhan Y, Hermosillo G, Babb J, Jelescu I O, Faul D, Boada F E and Shepherd T M 2016 Dixon Sequence with superimposed model-based bone compartment provides highly accurate PET/MR attenuation correction of the brain *J. Nucl. Med.* **57** 918–24

Nagarajah J, Jentzen W, Hartung V, Rosenbaum-Krumme S, Mikat C, Heusner T A, Antoch G, Bockisch A and Stahl A 2011 Diagnosis and dosimetry in differentiated thyroid carcinoma using 124I PET: comparison of PET/MRI versus PET/CT of the neck *Eur. J. Nucl. Med. Mol. Imaging* **38** 1862–8

Paulus D H, Braun H, Aklan B and Quick H H 2012 Simultaneous PET/MR imaging: MR-based attenuation correction of local radiofrequency surface coils *Med. Phys.* **39** 4306–15

Paulus D H, Quick H H, Geppert C, Fenchel M, Zhan Y, Hermosillo G, Faul D, Boada F, Friedman K P and Koesters T 2015 Whole-body PET/MR imaging: quantitative evaluation of a novel model-based MR attenuation correction method including bone *J. Nucl. Med.* **56** 1061–6

Preylowski V, Schlogl S, Schoenahl F, Jorg G, Samnick S, Buck A K and Lassmann M 2013 Is the image quality of I-124-PET impaired by an automatic correction of prompt gammas? *PLoS One* **8** e71729

Schulz V *et al* 2011 Automatic, three-segment, MR-based attenuation correction for whole-body PET/MR data *Eur. J. Nucl. Med. Mol. Imaging* **38** 138–52

Sgouros G, Kolbert K S, Sheikh A, Pentlow K S, Mum E F, Barth A, Robbins R J and Larson S M 2004 Patient-specific dosimetry for ^{131}I thyroid cancer therapy using 124I PET and 3-dimensional-internal dosimetry (3D-ID) software *J. Nucl. Med.* **45** 1366–72

Soderlund A T, Chaal J, Tjio G, Totman J J, Conti M and Townsend D W 2015 Beyond 18F-FDG: characterization of PET/CT and PET/MR scanners for a comprehensive set of positron emitters of growing application—18F, 11C, 89Zr, 124I, 68Ga, and 90Y *J. Nucl. Med.* **56** 1285–91

Wierts R, Brans B, Havekes B, Kemerink G, Halders S, Schaper N, Backes W, Mottaghy F M and Jentzen W 2016 Dose-response relationship in differentiated thyroid cancer patients undergoing radioiodine treatment assessed by means of ^{124}I PET/CT *J. Nucl. Med.* **57** 1027–32

Ziegler S, Jakoby B W, Braun H, Paulus D H and Quick H H 2015 NEMA image quality phantom measurements and attenuation correction in integrated PET/MR hybrid imaging *EJNMMI Phys.* **2** 18